Sensor applications

A Sensor Model to Simulate the Excitation and Propagation of Lamb Waves in Lithium-Ion Pouch Cells

Alexander Siegl* , Bernhard Schweighofer , and Hannes Wegleiter

Institute of Electrical Measurement and Sensor Systems, Graz University of Technology, 8010 Graz, Austria
**Graduate Student Member, IEEE*

Manuscript received 12 July 2023; accepted 26 July 2023. Date of publication 1 August 2023; date of current version 9 August 2023.

Abstract—The demand for lithium-ion battery cell monitoring is growing rapidly as the number of cells used in various applications increases. A novel monitoring approach is based on the mechanical properties of the battery, which change during the charge/discharge process and during its lifetime. In this approach, an acoustic wave is generated inside the battery by a transmitter and propagates through the layered structure of the cell to a receiver. The propagation speed of the wave changes depending on the mechanical properties of the cell, and so does the measurable time of flight between the transmitter and receiver. To apply this monitoring approach, it is essential to understand how this wave actually forms and travels through the individual layers. To improve this understanding, a model is presented that simulates both the generation and propagation of the wave within the battery. The model is parametrized by performing reference measurements and a tear down analysis of the battery. The simulation result shows good agreement with the measurement results and also provides a visualization of the acoustic wave motion within the cell, which greatly improves the understanding of the propagating wave.

Index Terms—Sensor applications, battery modeling, electromagnetic acoustic transducer (EMAT), Lamb mode propagation, lithium-ion pouch cell, nondestructive testing, sensor modeling.

I. INTRODUCTION

Lithium-ion batteries (LIBs) are commonly used in many applications today. Especially, in the automotive industry, single lithium-ion pouch cells are assembled to entire battery packs to power electric cars. In order to guarantee safety operation [1], those cells have to be properly monitored in terms of their state of charge (SoC) and state of health [2]. Besides the typical monitoring approaches where voltage, current, and temperature of the battery are measured [3], [4], [5], mechanical monitoring has recently become more popular [6]. A sketch of the setup for this approach is pictured in Fig. 1. An acoustic transmitter generates an acoustic wave inside the pouch cell. After a certain time of flight (ToF), the wave arrives at the receiver. Depending on the mechanical properties of the battery (e.g., stiffness), which change during charging/discharging and over the lifetime [7], [8], [9], the propagation velocity of the acoustic wave changes and, thus, so does the ToF [10], [11].

Although a battery is composed of many individual layers, as will be shown later, the pouch cell can be considered as a plate-like structure in the setup shown in Fig. 1. Within the cell, so-called Lamb waves (guided waves) are formed upon excitation [12], [13]. Siegl et al. [14] first showed the excitation and the propagation of a specific lamb mode, referred to as antisymmetric mode A_0, on a pouch cell. Koller et al. [15] then confirmed the excitation of this mode and pointed out that the propagation velocity of the A_0 mode varies from 60 to 140 m/s for the batteries measured, although the batteries were all of the same type. Moreover, depending on the excitation frequency and the thickness of the cell, several of these Lamb waves form simultaneously in the battery and overlap. This interference complicates the understanding of which layers within the cell are actually mechanically excited, and can contribute to a measurable change in ToF.

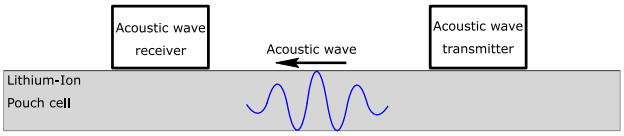

Fig. 1. Sketch of the mechanical monitoring approach for a lithium-ion pouch cells. A transmitter generates an acoustic wave inside the pouch cell. After a certain ToF, it arrives at the receiver.

In this letter, we introduce a model to simulate the excitation and propagation of an acoustic wave inside a LIB. The model includes the detailed layered structure of the battery and shows how the propagation velocity of the wave changes as the mechanical parameters of the battery change. In addition, the model provides a graphical illustration how the acoustic wave propagates inside the battery. This visualization greatly improves the understanding of how the single layers actually move when they are excited by a transmitter.

We consider this model as a starting point for further research and demonstrate its functionality as follows. In Section II, measurement experiments are performed to provide a reference for the model. Hereby, the antisymmetric mode A_0 is excited inside the cell. Section III includes a detailed description of the battery structure and its mechanical properties. In Section IV, the model is presented. The model is then parametrized accordingly to ensure that the simulation results match the reference measurements.

II. MEASUREMENT EXPERIMENTS

For the measurements, the cell is charged to 100% SoC. During the work, the SoC of the battery is not changed. The battery is used in

Corresponding author: Alexander Siegl (e-mail: alexander.siegl@tugraz.at).
Associate Editor: Jeong Bong (JB) Lee.
Digital Object Identifier 10.1109/LSENS.2023.3300805

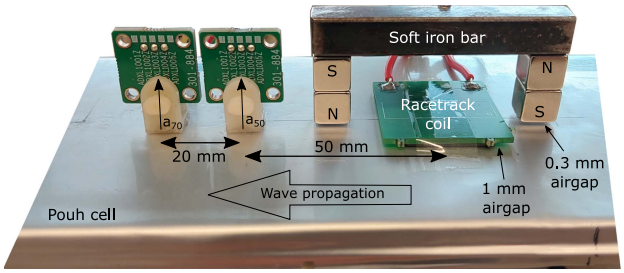

Fig. 2. Measurement setup to estimate the propagation velocity of the wave inside the pouch cell. An EMAT generates the acoustic wave and the out-of-plane acceleration is measured 50 and 70 mm from the EMAT.

two lab experiments where the zero-order antisymmetric mode A_0 is excited inside the battery with an electromagnetic acoustic transducer (EMAT) [16]. The purpose of these measurement experiments is to generate a reference for the simulation study and the corresponding parameterization of the battery model. Hereby, two different measurements are carried out.

A. Setup

The first measurement is a validation of the A_0 mode excitation. In this experiment, the out-of-plane acceleration is measured simultaneously on the top and bottom sides of the battery at a distance of 50 mm from the EMAT. The second experiment is intended to provide a rough estimation for the velocity of the propagating wave. The measurement setup for this experiment is shown in Fig. 2. The EMAT consists of a horseshoe permanent magnet, including the iron bar and cubic NdFeB magnets, and a racetrack coil centered below the permanent magnet. As shown in [14], this EMAT generates a Lorentz force excitation perpendicular to the battery surface. The racetrack coil is lifted 1 mm and the permanent magnet is lifted around 0.3 mm from the battery surface to demonstrate the excitation of acoustic waves without any contact between EMAT and battery. The EMAT is driven by a power amplifier (PA04) from Apex Microtechnology. It amplifies the Gaussian modulated excitation pulse with center frequency of 3 kHz, provided by a signal generator. The acceleration sensors (ADXL1005) used in the experiments are sensitive in one direction and have a cutoff frequency of 23 kHz. They are soldered onto an evaluation board and inserted into plastic sockets that are mechanically attached to the battery with beeswax. The acceleration sensors are placed 50 and 70 mm from the EMAT and measure the out-of-plane acceleration a_{50} and a_{70}, respectively. The measured acceleration signals are the average of 100 measurements.

B. Measurement Results

The result of the first experiment is shown in Fig. 3. In this figure, the Gaussian-modulated excitation current pulse and the measured accelerations at the top and bottom of the pouch cell are plotted at a distance of 50 mm from the EMAT. The reference point in time of 0 s is placed at the peak of the excitation pulse. The acceleration signals are normalized with respect to their maximum amplitude. As can be seen, the accelerations on top and bottom sides of the pouch cell show an in-phase behavior, meaning that at a certain point in time, the out-of-plane acceleration is the same. According to [12], such a characteristic indicates and verifies the propagation of the antisymmetric guided wave mode A_0 inside the battery. To determine the propagation velocity of the wave, the time difference

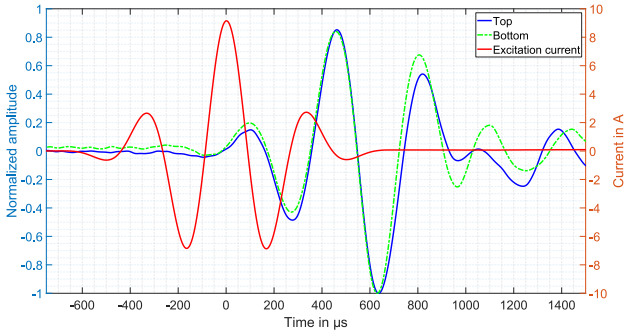

Fig. 3. Excitation current pulse and measured normalized acceleration on the top and bottom surface of the cell. The top and bottom signals show the in-phase characteristic and confirm the excitation of the A_0 mode inside the battery.

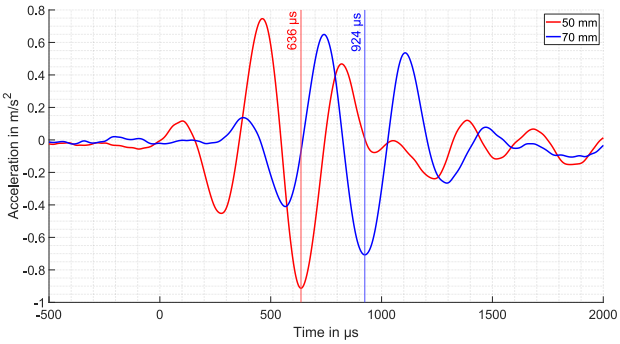

Fig. 4. Measured accelerations at distances 50 and 70 mm. A delay of 288 μs is determined between the two positions.

between the two minima in the measured acceleration signals at the distances 50 and 70 mm are evaluated. The measured accelerations and the corresponding evaluated times at the minimum acceleration are illustrated in Fig. 4. As can be seen, the wave first arrives at the 50 mm position and the minimum for the acceleration is found at 636 μs. As the wave propagates forward, it passes the accelerometer at the 70 mm position. The corresponding acceleration has its minimum at 924 μs. Given those points, a time delay of 288 μs is evaluated. The distance between the accelerometers is 20 mm, thus the wave propagates with a velocity of about 69 m/s.

The in-phase behavior seen in Fig. 3 and the measured delay evaluated from Fig. 4 serve as reference for the output of the simulation model.

III. BATTERY DATA

The battery used in this work is a LG CHEM E61 V pouch cell. The cell has a height of 10.7 mm, a length of 320 mm, and a width of 100 mm. As mentioned in the introduction, the goal of this work is to provide a simulation framework for acoustic wave propagation inside LIBs. Hereby, the model of the battery is crucial in terms of battery structure and material parameters.

A. Layer Structure

The battery itself is composed of multiple layers. Hereby, a basic stack consists of eight layers and is repeatedly stacked up until the desired capacity is reached. The layered sequence of the basic stack is shown in Fig. 5 (zoom of the first couple of layers). The basic stack

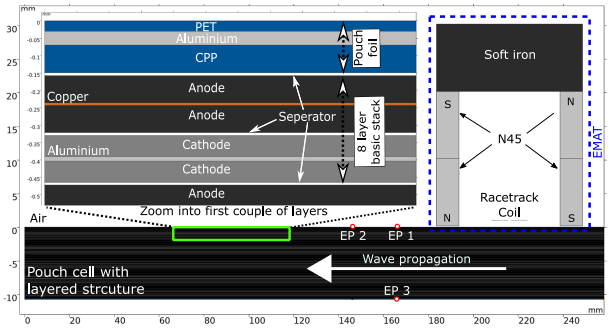

Fig. 5. 2-D model including the EMAT and the battery with its detailed layered structure to simulate the wave excitation and propagation. A zoom into the first couple of layers depicts the buildup of the basic stack. The out-of-plane acceleration is evaluated at the evaluation points EP1–EP3.

Table 1. Mechanical parameters of the pouch foil and the layers of the basic stack of the LIB

Material	Thickness [µm]	Young's Modulus [GPa]	Poisson's ratio	Density [kg/m^3]
PET	30	2.9 [17]	0.43 [18]	1200 [17]
Aluminum (Pouch foil)	40	70	0.345	2700
CPP	80	1.3 [17]	0.43 [18]	909 [17]
Aluminum	13	70	0.345	2700
Copper	8	100	0.3	8900
Anode	78	0.07 [19]	0.01 [15]	1842
Cathode	61	0.12 [19]	0.01 [15]	3630
Separator	8	0.35 [20]	0.4 [15]	1000 [15]

contains two layers of anode material. In between the anode material, there is a copper current collector. After the second anode layer, a thin separator layer is implemented. Then, there are two layers of cathode material. Between the cathode material, an aluminum current collector is inserted. The last layer of the basic stack is again a separator. This stack is then repeated as an anode layer follows the last separator of the basic stack. On the outside of the cell, a pouch foil is wrapped around. It consists of three single layers. A polyethylene terephthalate (PET) layer, an aluminum foil, and a layer of cast polypropylene (CPP). Between the pouch foil and the basic stack, a further layer of separator is inserted.

B. Tear Down Analysis

A detailed list of the single layer widths and their mechanical material properties is given in Table 1. The width of each layer and the density of the anode and cathode material results from a tear down analysis. Hereby, the cell was completely discharged, cut open, dried, and disassembled. The number of repeated basic stacks for the pouch cell is 33. After the drying process, the mass of the cell was about 140 g less than before drying. The difference in mass results from the evaporation of the electrolyte. This measured mass difference is divided in half and added to the mass of the anode or cathode material to calculate the associated densities. Material parameters for aluminum and copper were extracted from the material database of COMSOL-Multiphysics. The values for the remaining materials are from the listed references.The listed values serve as a starting point for the parameterization of the model.

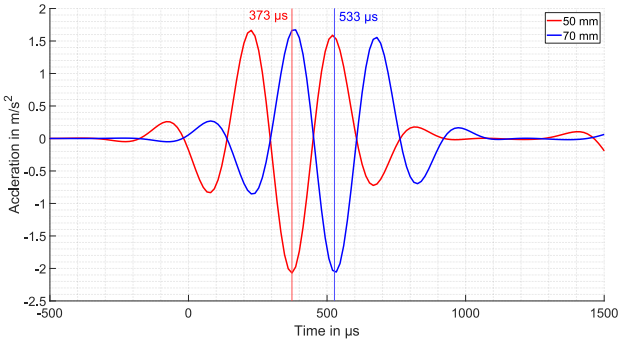

Fig. 6. Simulated accelerations at EP1 and EP2. The model is parametrized with the values of Table 1.

IV. 2-D SIMULATION MODEL

The model is created in COMSOL-Multiphysics. Within COMSOL, the *magnetic field*, the *Lorentz coupling*, and the *solid mechanics* modules are used to simulate the EMAT excitation, the Lorentz force generation, and the propagation of the guided wave inside the battery. The geometry of the model is pictured in Fig. 5. It includes the EMAT and the battery. The modeled EMAT is also lifted from the pouch cell surface in the same way as shown in the measurement setup in Fig. 2. The modeled pouch cell is created by a repeated buildup of the basic stack, which is zoomed out, as shown in Fig. 5. According to the tear down analysis, the basic stack is repeated 33 times, resulting in 264 single layers (without pouch foil). On the bottom side of the battery, the three layers of the pouch cell are implemented. The thickness of each layer is listed in Table 1. The resulting thickness of the battery model is 10.7 mm. As input signal serves again the 3 kHz Gaussian-modulated excitation current pulse through the coil. There are three evaluation points (EP1–EP3). EP1 and EP2 are placed on top of the battery. The distance from EP1 to the center of the EMAT is 50 mm. The distance between EP2 and EMAT is 70 mm. EP3 is located at the bottom surface of the battery, directly beneath EP1. At the evaluation points, the out-of-plane acceleration is evaluated, to get a direct comparison to the measured acceleration. The entire model geometry shown in Fig. 5 mimics the measurement setup in Fig. 2. In the following section, the model outputs, namely, the evaluated accelerations at EP1–EP3, are compared with the references from the measurements.

A. Simulation Results

In order to simulate the acoustic wave inside the battery, the single layers have to be assigned a Young's modulus, a Poisson's ratio, and a density. We assume that each material is homogeneous and isotropic. In a first step, the model is parametrized with the listed values from Table 1. The acceleration at the distances 50 and 70 mm is evaluated and plotted in Fig. 6. The simulation result shows a delay of 160 μs. Given the distance of 20 mm, that results in a propagation velocity of 125 m/s. Compared with the measured velocity of 69 m/s, the simulated velocity is too high. Given the model, one can now adjust the material properties. In particular, the Young's modulus of the anode and cathode material should be reconsidered, since the measurement in [19] is based on the measurement of a dry stack of anodes or cathodes, respectively. As the velocity is proportional with the Young's modulus, a reduction in Young's modulus of the anode and cathode material is, therefore, suggested. A good fit can be achieved by reducing the Young's modulus down to 30% of its initial value for both anode and cathode material. The corresponding

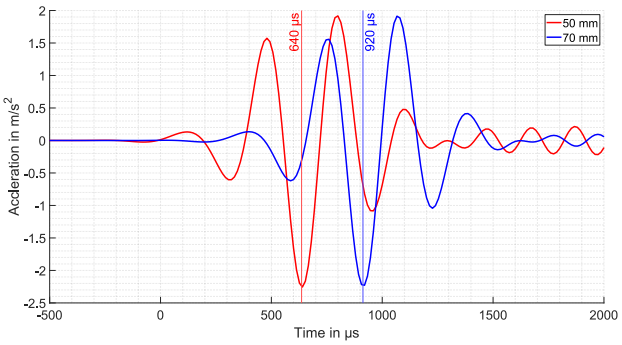

Fig. 7. Simulated accelerations at EP1 and EP2. The model is parametrized with 30% of Young's modulus for both anode and cathode material.

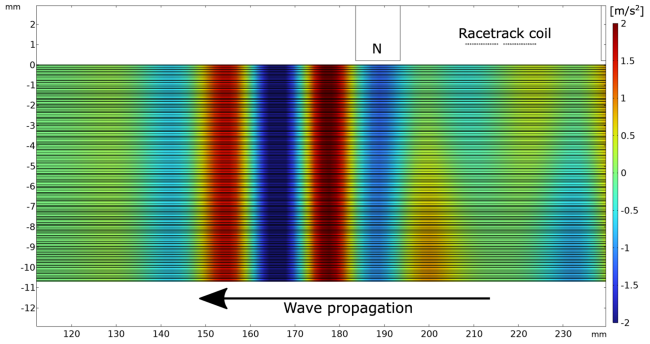

Fig. 8. Visualization of the simulated out-of-plane acceleration inside the LIB at 640 μs. The color denotes the amplitude of acceleration.

simulated accelerations are plotted in Fig. 7. As can be seen, the calculated delay equals 280 μs. For the given distance of 20 mm, a propagation velocity of about 71 m/s is achieved. Thus, by reducing the Young's modulus, we already achieve a good agreement with the measurement in Fig. 4. Although, the propagation velocity between measurement and simulation agrees well, there is still difference in the amplitude of the accelerations. The simulated amplitude is roughly two times higher compared with the measured amplitudes. This indicates a damping inside the LIB, which is not yet considered in the model and is seen as future work. After adjusting the Young's modulus to match the propagation velocity, also the behavior of the simulated wave movement inside the battery can be evaluated. A visualization of the simulated out-of-plane acceleration is depicted in Fig. 8. As can be seen, all the layers inside the battery move in-phase and show the modulation pattern of the excitation pulse. An evaluation of the acceleration at EP1 and EP3 would then match the measurement result in Fig. 3.

V. CONCLUSION

It was possible to develop a model that fits the measured results very well. Thus, the model can serve as a basic framework for a number of further possible investigations. For example, sensitivity analyses can be performed with respect to the mechanical parameters. In addition, the influence of the transmitter and its excitation of the acoustic wave inside the battery can be analyzed, allowing the search for an optimal setup for mechanical excitation of the battery. Furthermore, the model provides a visualization of the wave motion inside the battery, which greatly improves the understanding of the propagating waves in each layer of the battery.

ACKNOWLEDGMENT

This work was supported in part by the Austrian Research Promotion Agency (FFG) under Grant #879610 and in part by the TU Graz Open Access Publishing Fund, Austria.

REFERENCES

[1] M. Kaliaperumal et al., "Cause and mitigation of lithium-ion battery failure—A review," *Materials*, vol. 14, p. 2021, Art. no. 5676.
[2] W. Waag, C. Fleischer, and D. U. Sauer, "Critical review of the methods for monitoring of lithium-ion batteries in electric and hybrid vehicles," *J. Power Sources*, vol. 258, pp. 321–339, 2014.
[3] S. Zhu et al., "A novel embedded method for in-situ measuring internal multi-point temperatures of lithium ion batteries," *J. Power Sources*, vol. 456, 2020, Art. no. 227981.
[4] X. Hu, J. Jiang, D. Cao, and B. Egardt, "Battery health prognosis for electric vehicles using sample entropy and sparse Bayesian predictive modeling," *IEEE Trans. Ind. Electron.*, vol. 63, no. 4, pp. 2645–2656, Apr. 2016.
[5] L. Lu, X. Han, J. Li, J. Hua, and M. Ouyang, "A review on the key issues for lithium-ion battery management in electric vehicles," *J. Power Sources*, vol. 226, pp. 272–288, 2013.
[6] H. Popp, M. Koller, M. Jahn, and A. Bergmann, "Mechanical methods for state determination of lithium-ion secondary batteries: A review," *J. Energy Storage*, vol. 32, 2020, Art. no. 101859.
[7] G. Davies et al., "State of charge and state of health estimation using electrochemical acoustic time of flight analysis," *J. Electrochem. Soc.*, vol. 164, pp. A2746–A2755, 2017.
[8] L. Gold et al., "Probing lithium-ion batteries' state-of-charge using ultrasonic transmission, concept and laboratory testing," *J. Power Sources*, vol. 343, pp. 536–544, 2017.
[9] J. B. Robinson, M. Pham, M. D. R. Kok, T. M. M. Heenan, D. J. L. Brett, and P. R. Shearing, "Examining the cycling behaviour of li-ion batteries using ultrasonic time-of-flight measurements," *J. Power Sources*, vol. 444, 2019, Art. no. 227318.
[10] H. Popp, M. Koller, S. Keller, G. Glanz, R. Klambauer, and A. Bergmann, "State estimation approach of lithium-ion batteries by simplified ultrasonic time-of-flight measurement," *IEEE Access*, vol. 7, pp. 170992–171000, 2019.
[11] Y. Wu, Y. Wang, W. K. C. Yung, and M. Pecht, "Ultrasonic health monitoring of lithium-ion batteries," *Electronics*, vol. 8, 2019, Art. no. 751.
[12] J. L. Rose, *Ultrasonic Guided Waves in Solid Media*. Cambridge, U.K.: Cambridge Univ. Press, 2014.
[13] P. Ladpli, F. Kopsaftopoulos, and F.-K. Chang, "Estimating state of charge and health of lithium-ion batteries with guided waves using built-in piezoelectric sensors/actuators," *J. Power Sources*, vol. 384, pp. 342–354, 2018.
[14] A. Siegl, B. Schweighofer, A. Bergmann, and H. Wegleiter, "An electromagnetic acoustic transducer for generating acoustic waves in lithium-ion pouch cells," in *Proc. IEEE Int. Instrum. Meas. Technol. Conf.*, 2022, pp. 1–6.
[15] M. Koller, G. Glanz, A. Bergmann, and H. Popp, "Determination of lamb wave modes on lithium-ion batteries using piezoelectric transducers," *Sensors*, vol. 22, no. 13, 2022, Art. no. 4748.
[16] M. Hirao and H. Ogi, *Electromagnetic Acoustic Transducers*. Tokyo, Japan: Springer, 2017.
[17] Designerdata, "Thermo plastics," 2022. Accessed: Jun. 15, 2023. [Online]. Available: https://designerdata.nl/materials/plastics/thermo-plastics
[18] Polymerdatabase, "Typical poisson's ratios of polymers at room temperature," 2022. Accessed: Jun. 15, 2023. [Online]. Available: http://polymerdatabase.com/polymer%20physics/Poisson%20Table.html
[19] M. Nikpour, N. Barrett, Z. Hillman, A. Thompson, B. Mazzeo, and D. Wheeler, "A model for investigating sources of Li-ion battery electrode heterogeneity: Part I. electrode drying and calendering processes," *J. Electrochem. Soc.*, vol. 168, no. 6, 2021, Art. no. 060547.
[20] G. Y. Gor, J. Cannarella, J. H. Prévost, and C. B. Arnold, "A model for the behavior of battery separators in compression at different strain/charge rates," *J. Electrochem. Soc.*, vol. 161, no. 11, 2014, Art. no. F3065.